

# New physics effects on $B \rightarrow D^{(*)}\tau\nu$ decays

Jong-Phil Lee\*

*Sang-Huh College, Konkuk University, Seoul 05029, Korea*

## Abstract

We investigate new physics effects on  $B \rightarrow D^{(*)}\tau\nu$  decays in a general and model-independent way. The  $\chi^2$  fits for fractions of the branching ratios  $R(D^{(*)})$  and other polarization parameters are implemented. We parameterize the relevant Wilson coefficients with a new physics scale and its power together with combined fermionic couplings. Constraints from  $B_c \rightarrow \tau\nu$  are imposed such that its branching ratio is less than 30%. For a moderate range of our parameters we find that the new physics scale goes up to  $\lesssim 27$  TeV for ordinary new particle contributions. It turns out that the polarization asymmetry of  $\tau$  for  $B \rightarrow D$  transition can be negative only for a few combinations of the new physics operators. We also discuss related processes  $B_c \rightarrow J/\Psi\tau\nu$  and  $\Lambda_b \rightarrow \Lambda_c\tau\nu$  decays.

---

\* jongphil7@gmail.com

## I. INTRODUCTION

The standard model (SM) is an important cornerstone of today's particle physics. It has been very successful for many decades since its advent. On the other hand, we know that there must be some new physics (NP) beyond the SM. Flavor physics plays a very important role in probing NP. Recently various decay modes of  $B$  showed some anomalies which deviate from the SM predictions.

Among them is the ratio of  $R(D^{(*)})$  in  $b \rightarrow c$  transition, which is defined by

$$R(D^{(*)}) \equiv \frac{\text{Br}(B \rightarrow D^{(*)}\tau\nu)}{\text{Br}(B \rightarrow D^{(*)}\ell\nu)} , \quad (1)$$

where  $\ell = \mu$  or  $e$ . For  $b \rightarrow s$  transition we have similar ratios  $R(K^{(*)})$ . Recent measurements from LHCb turn out to be consistent with the SM [1, 2], alleviating a tension between experiment and theory. Unlike  $R(K^{(*)})$ ,  $R(D^{(*)})$  involves charged currents and the processes occur at tree level in the SM.

Besides the fraction of the branching ratios there also exist polarization parameters. The polarization asymmetry of  $\tau$  is defined as

$$P_\tau(D^{(*)}) \equiv \frac{\Gamma_\tau^{D^{(*)}}(+)-\Gamma_\tau^{D^{(*)}}(-)}{\Gamma_\tau^{D^{(*)}}(+)+\Gamma_\tau^{D^{(*)}}(-)} , \quad (2)$$

where  $\Gamma_\tau^{D^{(*)}}(\pm)$  is the decay width corresponding to  $(\pm)$   $\tau$  helicity.

As for  $D^*$  we can define the longitudinal polarization as

$$F_L(D^*) \equiv \frac{\Gamma(B \rightarrow D_L^*\tau\nu)}{\Gamma(B \rightarrow D^*\tau\nu)} . \quad (3)$$

The SM predictions for these observables are [3, 4]

$$R(D)_{\text{SM}} = 0.290 \pm 0.003 , \quad (4)$$

$$R(D^*)_{\text{SM}} = 0.248 \pm 0.001 , \quad (5)$$

$$P_\tau(D)_{\text{SM}} = 0.331 \pm 0.004 , \quad (6)$$

$$P_\tau(D^*)_{\text{SM}} = -0.497 \pm 0.007 , \quad (7)$$

$$F_L(D^*)_{\text{SM}} = 0.464 \pm 0.003 . \quad (8)$$

Experimentally, there are some tensions compared with the SM predictions. Very recent data from the LHCb tell that [5]

$$R(D) = 0.249 \pm 0.043 \pm 0.047 , \quad R(D^*) = 0.402 \pm 0.081 \pm 0.085 . \quad (9)$$

The polarization asymmetry was measured to be [6, 7]

$$P_\tau(D^*) = -0.38 \pm 0.51^{+0.21}_{-0.16} . \quad (10)$$

Recent measurement of the longitudinal  $D^*$  polarization by the LHCb is [8]

$$F_L(D^*) = 0.43 \pm 0.06 \pm 0.03 . \quad (11)$$

The value is closer to the SM prediction of Eq. (8) than the previous measurements  $F_L(D^*) = 0.60 \pm 0.08 \pm 0.04$  by Belle [9]. But other observables, especially  $R(D^*)$ , strongly imply that there might be NP to affect the  $B \rightarrow D^{(*)}\tau\nu$  decay.

There have been many NP scenarios suggested to explain the  $B$  anomalies, including leptoquarks (LQ) [10–14],  $W'$  [15–18], charged Higgs [19–21], or unparticles [22]. All of these NP effects occur via tree-level contributions with charged currents.

In this paper we investigate the NP effects in a more general way. We parametrized the NP contributions as new Wilson coefficients  $C_j^{\text{NP}} \sim A_j(v/M_{\text{NP}})^\alpha \left[ \alpha_s(M_{\text{NP}}) \right]^{\gamma_j/2\beta_0^{(n_f)}}$  where  $M_{\text{NP}}$  is the NP scale,  $v$  is the SM vacuum expectation value,  $\gamma_j$  is the anomalous dimension, and  $\beta_0^{(n_f)} = 11 - 2n_f/3$  with  $n_f$  being the number of quark flavors. Terms with  $\alpha_s(M_{\text{NP}})$  reflect the renormalization group (RG) running effects. We allow  $\alpha$  to be a free parameter inspired by the unparticle scenario. The case where  $\alpha = 2$  corresponds to ordinary new particle contributions at tree level such as LQ,  $W'$ , or charged Higgs, etc. Other details of NP models are encapsulated in the coefficients  $A_j$ . In this framework the interplay between the fermionic coupling and the new mediator for NP contributions can be easily seen. For some specific NP models if the allowed range of the relevant couplings and the mass scale of the new mediating (un)particle were known from other processes, then one could check directly the compatibility of the model with  $B \rightarrow D^{(*)}\tau\nu$  with the help of our analysis. The approach was applied to  $R(K^{(*)})$  previously [23, 24]. One can examine general features of NP effects on  $B \rightarrow D^{(*)}\tau\nu$  decays in model-independent ways.

Closely related observables are  $R(J/\Psi)$  and  $R(\Lambda_c)$ . They are defined by

$$R(J/\Psi) = \frac{\text{Br}(B_c \rightarrow J/\Psi\tau\nu)}{\text{Br}(B_c \rightarrow J/\Psi\mu\nu)} , \quad (12)$$

$$R(\Lambda_c) = \frac{\text{Br}(\Lambda_c \rightarrow \tau\nu)}{\text{Br}(\Lambda_c \rightarrow \ell\nu)} . \quad (13)$$

Especially it is known that  $R(\Lambda_c)$  satisfies a sum rule with respect to  $R(D^{(*)})$  as [25–27]

$$\frac{R(\Lambda_c)}{R(\Lambda_c)_{\text{SM}}} \simeq 0.280 \frac{R(D)}{R(D)_{\text{SM}}} + 0.720 \frac{R(D^*)}{R(D^*)_{\text{SM}}} . \quad (14)$$

The SM predicts that  $R(J/\Psi)_{\text{SM}} = 0.258 \pm 0.004$  [28] and  $R(\Lambda_c)_{\text{SM}} = 0.324 \pm 0.004$  [29, 30]. Recent experimental data reveal some tension with the SM results as  $R(J/\Psi) = 0.61 \pm 0.18$  [4] and  $R(\Lambda_c) = |0.04/V_{cb}|^2(0.285 \pm 0.073)$  [31]. NP effects, if exist, seems to enhance  $R(J/\Psi)$  while shrink  $R(\Lambda_c)$ . Still there exist large experimental uncertainties for both of them and we will not take  $R(J/\Psi)$  and  $R(\Lambda_c)$  as fitting data. Instead we provide outlooks of NP effects allowed by  $B \rightarrow D^{(*)}$  transitions on them.

The branching ratio of  $\text{Br}(B_c \rightarrow \tau\nu)$  puts constraints on NP contributions. We require a moderate bound of the branching ratio as  $\text{Br}(B_c \rightarrow \tau\nu) < 0.3$  [32]. As will be seen later, most of allowed branching ratios of our analysis are safely below the bound.

The paper is organized as follows. In Sec. II we give the setup for our analysis. Relevant observables are described by Wilson coefficients with our new parametrization. Our results and related discussions will appear in Sec. III. Section IV provides conclusions and outlooks.

## II. SETUP

Let's start with the  $b \rightarrow c$  transition. The effective Hamiltonian for  $b \rightarrow c\ell\nu$  is

$$\mathcal{H}_{\text{eff}} = \frac{4G_F}{\sqrt{2}}V_{cb} \sum_{\ell=\mu,\tau} [(1 + C_{VL}^\ell)\mathcal{O}_{VL}^\ell + C_{SL}^\ell\mathcal{O}_{SL}^\ell + C_{SR}^\ell\mathcal{O}_{SR}^\ell + C_T^\ell\mathcal{O}_T^\ell] , \quad (15)$$

where the operators  $\mathcal{O}_{V,S}^\ell$  are defined by

$$\mathcal{O}_{VL}^\ell = (\bar{c}_L\gamma^\mu b_L)(\bar{\ell}_L\gamma_\mu\nu_{\ell L}) , \quad (16)$$

$$\mathcal{O}_{SL}^\ell = (\bar{c}_R b_L)(\bar{\ell}_R\nu_{\ell L}) , \quad (17)$$

$$\mathcal{O}_{SR}^\ell = (\bar{c}_L b_R)(\bar{\ell}_R\nu_{\ell L}) , \quad (18)$$

$$\mathcal{O}_T^\ell = (\bar{c}_R\sigma^{\mu\nu}b_L)(\bar{\ell}_R\sigma_{\mu\nu}\nu_{\ell L}) . \quad (19)$$

In our analysis the operator  $\mathcal{O}_{VR}^\ell = (\bar{c}_R\gamma^\mu b_R)(\bar{\ell}_L\gamma_\mu\nu_{\ell L})$  is neglected for simplicity. We assume that NP effects appear only in the  $\tau$  sector, so from now on we omit the superscript  $\ell$  of the operators and the Wilson coefficients in Eq. (15).

The observables for  $B \rightarrow D^{(*)}\tau\nu_\tau$  decays can be described numerically in terms of NP Wilson coefficients. We adopt recently updated formulae for the observables as follows (at

$\mu = \mu_b = 4.18 \text{ GeV scale})$  [4, 25, 33, 34]

$$\frac{R(D)}{R(D)_{\text{SM}}} = |1 + C_{VL}|^2 + 1.01|C_{SL} + C_{SR}|^2 + 0.84|C_T|^2 + 1.49\text{Re}[(1 + C_{VL})(C_{SL} + C_{SR})^*] + 1.08\text{Re}[(1 + C_{VL})C_T^*] , \quad (20)$$

$$\frac{R(D^*)}{R(D^*)_{\text{SM}}} = |1 + C_{VL}|^2 + 0.04|C_{SL} - C_{SR}|^2 + 16.0|C_T|^2 - 0.11\text{Re}[(1 + C_{VL})(C_{SL} - C_{SR})^*] - 5.17\text{Re}[(1 + C_{VL})C_T^*] , \quad (21)$$

and

$$\frac{P_\tau(D)}{P_\tau(D)_{\text{SM}}} = \left[ \frac{R(D)}{R(D)_{\text{SM}}} \right]^{-1} \left\{ |1 + C_{VL}|^2 + 3.04|C_{SL} + C_{SR}|^2 + 0.17|C_T|^2 + 4.50\text{Re}[(1 + C_{VL})(C_{SL} + C_{SR})^*] - 1.09\text{Re}(1 + C_{VL})C_T^* \right\} , \quad (22)$$

$$\frac{P_\tau(D^*)}{P_\tau(D^*)_{\text{SM}}} = \left[ \frac{R(D^*)}{R(D^*)_{\text{SM}}} \right]^{-1} \left\{ |1 + C_{VL}|^2 - 0.07|C_{SL} - C_{SR}|^2 - 1.85|C_T|^2 + 0.23\text{Re}[(1 + C_{VL})(C_{SL} - C_{SR})^*] - 3.47\text{Re}[(1 + C_{VL})C_T^*] \right\} , \quad (23)$$

$$\frac{F_L(D^*)}{F_L(D^*)_{\text{SM}}} = \left[ \frac{R(D^*)}{R(D^*)_{\text{SM}}} \right]^{-1} \left\{ |1 + C_{VL}|^2 + 0.08|C_{SL} - C_{SR}|^2 + 6.90|C_T|^2 - 0.25\text{Re}[(1 + C_{VL})(C_{SL} - C_{SR})^*] - 4.30\text{Re}[(1 + C_{VL})C_T^*] \right\} , \quad (24)$$

As for  $B_c \rightarrow J/\Psi \tau \nu$  and  $\Lambda_b \rightarrow \Lambda_c \tau \nu$  decays, we have [4]

$$\frac{R(J/\Psi)}{R(J/\Psi)_{\text{SM}}} = |1 + C_{VL}|^2 + 0.04|C_{SL} - C_{SR}|^2 - 0.10\text{Re}[(1 + C_{VL})(C_{SL} - C_{SR})^*] - 5.39\text{Re}[(1 + C_{VL})C_T^*] + 14.7|C_T|^2 , \quad (25)$$

$$\frac{R(\Lambda_c)}{R(\Lambda_c)_{\text{SM}}} = |1 + C_{VL}|^2 + 0.32(|C_{SL}|^2 + |C_{SR}|^2) + 0.52\text{Re}[C_{SL}C_{SR}^*] + 0.50\text{Re}[(1 + C_{VL})C_{SR}^*] + 0.33\text{Re}[(1 + C_{VL})C_{SL}^*] - 3.11\text{Re}[(1 + C_{VL})C_T^*] + 10.4|C_T|^2 . \quad (26)$$

Now the Wilson coefficients can be written as [10]

$$C_j(\mu_b) \equiv A_j \left( \frac{v}{M_{\text{NP}}} \right)^\alpha \left[ \frac{\alpha_s(m_t)}{\alpha_s(\mu_b)} \right]^{\frac{\gamma_j}{2\beta_0^{(5)}}} \left[ \frac{\alpha_s(M_{\text{NP}})}{\alpha_s(m_t)} \right]^{\frac{\gamma_j}{2\beta_0^{(6)}}} , \quad (27)$$

where  $A_j$  are some combinations of the relevant fermionic couplings of NP with  $j = VL, SL, SR, T$ , and  $M_{\text{NP}}$  is the NP scale. The exponent  $\alpha$  is taken to be a free parameter.

Terms with  $\alpha_s$  are for the RG running effects. More explicitly, we have [14]

$$C_{VL} = A_{VL} \left( \frac{v}{M_{\text{NP}}} \right)^\alpha, \quad (28)$$

$$C_{SL(R)} = A_{SL(R)} \left( \frac{v}{M_{\text{NP}}} \right)^\alpha \left[ \frac{\alpha_s(m_t)}{\alpha_s(\mu_b)} \right]^{-\frac{12}{23}} \left[ \frac{\alpha_s(M_{\text{NP}})}{\alpha_s(m_t)} \right]^{-\frac{4}{7}}, \quad (29)$$

$$C_T = A_T \left( \frac{v}{M_{\text{NP}}} \right)^\alpha \left[ \frac{\alpha_s(m_t)}{\alpha_s(\mu_b)} \right]^{\frac{4}{23}} \left[ \frac{\alpha_s(M_{\text{NP}})}{\alpha_s(m_t)} \right]^{\frac{4}{21}}, \quad (30)$$

$$(31)$$

where vector current Wilson coefficients do not run.

For example, contributions from the weak singlet scalar leptoquark are [3]

$$A_{SL} = -\frac{y_{1b\tau}^{LL}(y_{1c\tau}^{RR*})}{2V_{cb}}, \quad (32)$$

$$A_{VL} = \frac{y_{1b\tau}^{LL}(Vy_1^{LL*})_{c\tau}}{2V_{cb}}, \quad (33)$$

where  $V$  is the CKM matrix and  $y_{1ij}$  are the relevant couplings. Other NP models involve similar contributions.

The branching ratio of  $B_c \rightarrow \tau\nu$  is also directly related to  $C_{ij}$  as [3, 4]

$$\text{Br}(B_c \rightarrow \tau\nu) = \text{Br}(B_c \rightarrow \tau\nu)_{\text{SM}} \left| 1 + C_{VL} - 4.35(C_{SL} - C_{SR}) \right|^2, \quad (34)$$

where  $\text{Br}(B_c \rightarrow \tau\nu)_{\text{SM}} = 0.022$ . We require a moderate bound of  $\text{Br}(B_c \rightarrow \tau\nu) < 0.3$ .

### III. RESULTS AND DISCUSSIONS

Experimental data used for our fit are summarized in Table I. The  $\chi^2$  is defined by

$$\chi^2 \equiv \sum_{i,j} [\mathcal{O}_i^{\text{exp}} - \mathcal{O}_i^{\text{th}}] \mathcal{C}_{ij}^{-1} [\mathcal{O}_j^{\text{exp}} - \mathcal{O}_j^{\text{th}}], \quad (35)$$

where  $\mathcal{O}_i^{\text{exp}}$  are the experimental data in Table I and  $\mathcal{O}_i^{\text{th}}$  are the theoretical calculations from Eqs.(20)-(24). Here  $\mathcal{C}_{ij}$  are the correlation matrix elements.

The fitting parameters scan the range of  $0 \leq \alpha \leq 7$ ,  $1 \text{ TeV} \leq M_{\text{NP}} \leq 100 \text{ TeV}$ , and  $-100 \leq A_{ij} \leq 100$ . Our best-fit values are given in Table II. We have  $\chi_{\text{min}}^2/\text{d.o.f.} = 1.251$ . Note that the best-fit value of  $\alpha$  is slightly larger than ordinary value of 2, but the value of  $\chi^2$  at  $\alpha = 2$  is not so different from  $\chi_{\text{min}}^2$ .

Figure 1 shows the allowed region of  $\alpha$  vs.  $M_{\text{NP}}$  at the  $2\sigma$  level. For larger values of

	$R(D)$	$R(D^*)$
BABAR	$0.440 \pm 0.058 \pm 0.042$	$0.332 \pm 0.024 \pm 0.018$ [35]
Belle(2015)	$0.375 \pm 0.064 \pm 0.026$	$0.293 \pm 0.038 \pm 0.015$ [36]
Belle(2016)	—	$0.302 \pm 0.030 \pm 0.011$ [37]
Belle(2017)	—	$0.276 \pm 0.034^{+0.029}_{-0.026}$ [38]
Belle(2017)	—	$0.270 \pm 0.035^{+0.028}_{-0.025}$ [6, 7]
Belle(2019)	$0.307 \pm 0.037 \pm 0.016$	$0.283 \pm 0.018 \pm 0.014$ [39]
BelleII(2024)	—	$0.262^{+0.041+0.035}_{-0.039-0.032}$ [40]
LHCb(2015)	—	$0.336 \pm 0.027 \pm 0.030$ [41]
LHCb(2017)	—	$0.291 \pm 0.019 \pm 0.026 \pm 0.013$ [42]
LHCb(2023)	—	$0.260 \pm 0.015 \pm 0.016 \pm 0.012$ [43]
LHCb(2024)	$0.249 \pm 0.043 \pm 0.047$	$0.402 \pm 0.081 \pm 0.085$ [5]
	$P_\tau(D^*)$	$F_L(D^*)$
Belle(2017)	$-0.38 \pm 0.51^{+0.21}_{-0.16}$ [6, 7]	—
Belle(2019)	—	$0.60 \pm 0.08 \pm 0.04$ [9]
LHCb(2023)	—	$0.43 \pm 0.06 \pm 0.03$ [8]

TABLE I. Summary of experimental data for  $R(D^{(*)})$ ,  $P_\tau(D^{(*)})$  and  $F_L(D^*)$ . The uncertainties are  $\pm(\text{statistical})\pm(\text{systematic})$ . The correlations between  $R(D)$  and  $R(D^*)$  for BABAR, Belle(2015), Belle(2019), and LHCb(2024) results are  $-0.31$ ,  $-0.50$ ,  $-0.51$ , and  $-0.39$ , respectively [5, 44].

$M_{\text{NP}}$  the smaller values of  $\alpha$  are allowed. The horizontal red line corresponds to  $\alpha = 2$ . In our parameter space of  $-100 \leq A_j \leq 100$  the maximum value of  $M_{\text{NP}}$  is about 27 TeV for  $\alpha = 2$ . Of course the maximum  $M_{\text{NP}}$  could be larger for wider ranges of  $A_j$ . For example, if  $|A_j| \leq 200$  then  $M_{\text{NP}}$  can be as large as  $\sim 27 \times \sqrt{2} \simeq 38$  (TeV).

Actually direct search of  $M_{\text{NP}} = 27$  TeV is out of reach for current accelerators. To the extent that the logarithmic dependence of the RG running on  $M_{\text{NP}}$  is negligible, if  $A_j$  gets larger (smaller)  $k$  times then  $M_{\text{NP}}$  can be as large (small) as  $\sqrt{k}$  times. For example if  $k = 0.1$  then  $M_{\text{NP}}$  is roughly  $M_{\text{NP}} \lesssim 8.5$  TeV. In this way current accelerator could check the validity of NP models with small fermionic couplings.

In the unparticle scenario  $\alpha$  can be non-integer and  $M_{\text{NP}}$  is very sensitive to  $\alpha$ . For scalar (vector) unparticles  $\alpha$  can span  $2(4) \leq \alpha$  [22]. In case of  $\alpha = 4$ , we have  $M_{\text{NP}} \lesssim 2.52$  TeV.

$\alpha$	2.278	$R(D)$	0.329
$M_{\text{NP}}$	4.731(\text{TeV})	$R(D^*)$	0.291
$C_{VL}$	0.105	$P_\tau(D)$	0.258
$C_{SL}$	-0.188	$P_\tau(D^*)$	-0.454
$C_{SR}$	0.121	$F_L(D^*)$	0.490
$C_T$	-0.016	$\text{Br}(B_c \rightarrow \tau \nu)$	0.132

TABLE II. Best-fit values.

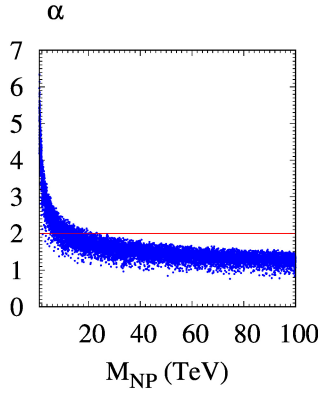


FIG. 1. Allowed regions of  $\alpha$  vs.  $M_{NP}$  at the  $2\sigma$  level.

If there were no unparticle signals below  $\sim 2.52$  TeV with  $|A_j| \leq 100$ , then the vector unparticle scenario would be disfavored.

In Fig. 2 we plot allowed regions of  $C_j$  with respect to  $\alpha$ . Around  $\alpha \approx 1$ ,  $|C_j|$ s can cover wider range, and attenuate as  $\alpha$  gets larger. Though our best-fit value of  $\alpha$  is around  $\sim 2$ ,  $\alpha$  can have  $\alpha \gtrsim 6$  as shown in the Figure. But in our parameter space,  $\alpha$  has an upper bound as  $\alpha \lesssim 6.4$ . Limiting case of  $\alpha \rightarrow \infty$  corresponds to the SM. The fact that  $\alpha$  has an upper bound tells that finite NP effects must exist to accommodate the experimental data; NP effects should not be suppressed so much.

Note that allowed values of  $|C_T|$  are smaller than other  $|C_{VL,SL,SR}|$  values. The reason is that the coefficients of  $C_T$  in Eqs. (20)-(24) are quite larger than those of any other  $C_j$ s. Explicitly, we have  $-0.186 \leq C_T \leq 0.278$ , while  $-0.568 \leq C_{VL} \leq 0.431$ ,  $-1.000 \leq C_{SL} \leq 0.761$ , and  $-1.123 \leq C_{SR} \leq 0.474$ .

Figure 3 shows the allowed regions of various observables,  $R(D^{(*)})$ ,  $P_\tau(D^{(*)})$ ,  $F_L(D^*)$ , and



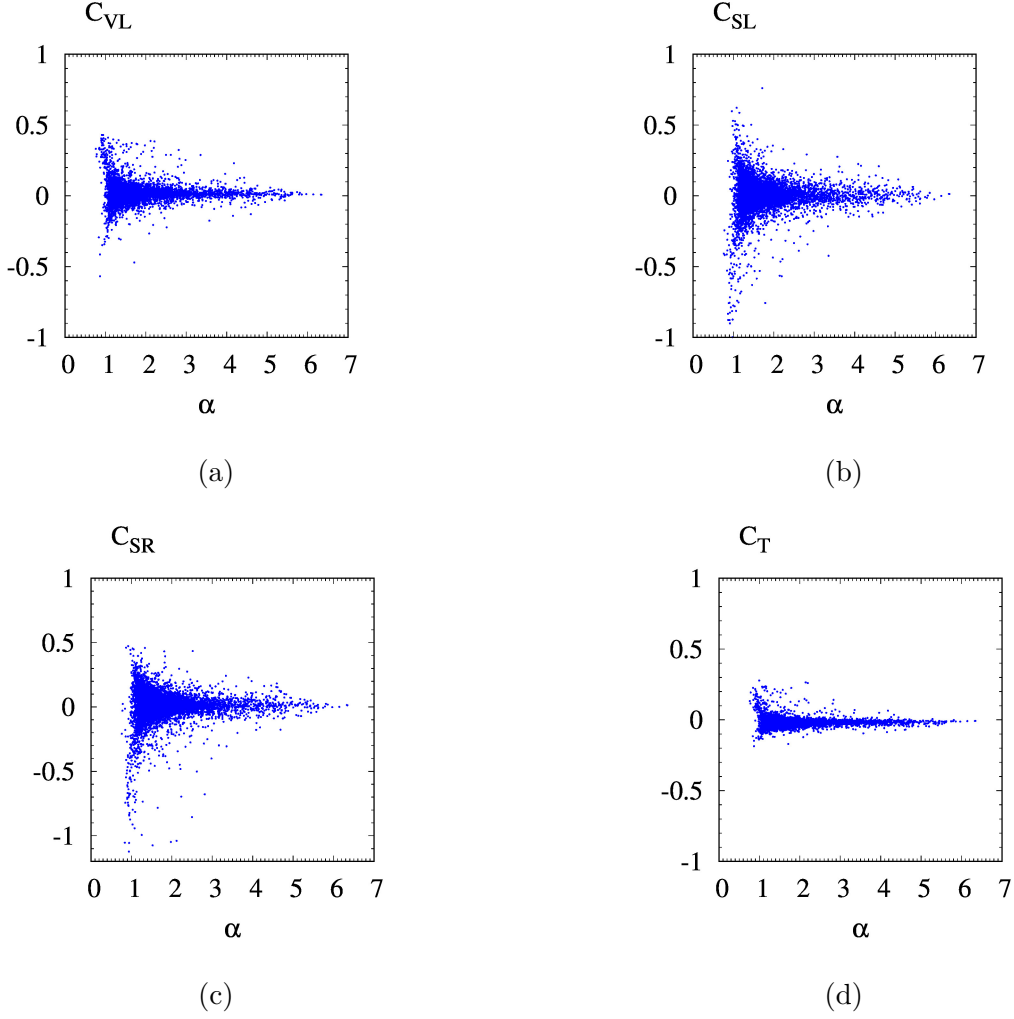


FIG. 2. Allowed regions of (a)  $C_{VL}$ , (b)  $C_{SL}$ , (c)  $C_{SR}$ , and  $C_T$  vs.  $\alpha$ , respectively, at the  $2\sigma$  level.

$\text{Br}(B_c \rightarrow \tau\nu)$ , with respect to  $\alpha$ . As in Fig. 2, these observables span wider range for  $\alpha \sim 1$ . As can be seen in Fig. 3 (a) and (b),  $R(D)$ ,  $P_\tau(D^{(*)})$ ,  $F_L(D^*)$ , and  $\text{Br}(B_c \rightarrow \tau\nu)$  tends to converge to the SM predictions as  $\alpha$  gets larger in our fittings. But  $R(D^*)$  values are still deviated from the SM prediction for large  $\alpha$ . It reflects the fact that  $R(D^*)$  data are farther from the SM value. In Fig. 3 (b) one can find that our fits have much more plots in positive  $P_\tau(D)$  than negative ones, but negative  $P_\tau(D)$  is also possible. The SM prediction for  $P_\tau(D)$  is positive definite as given in Eq. (6), so the observation of negative  $P_\tau(D)$  would strongly suggest the existence of NP. This is quite different from the unparticle scenario results. In Ref. [22] it was shown that unparticle contributes to produce positive  $P_\tau(D)$  (see Fig. 2(c) therein).

When turning on and off various combinations of  $C_{VL,SL,SR,T}$ , we find that only two cases

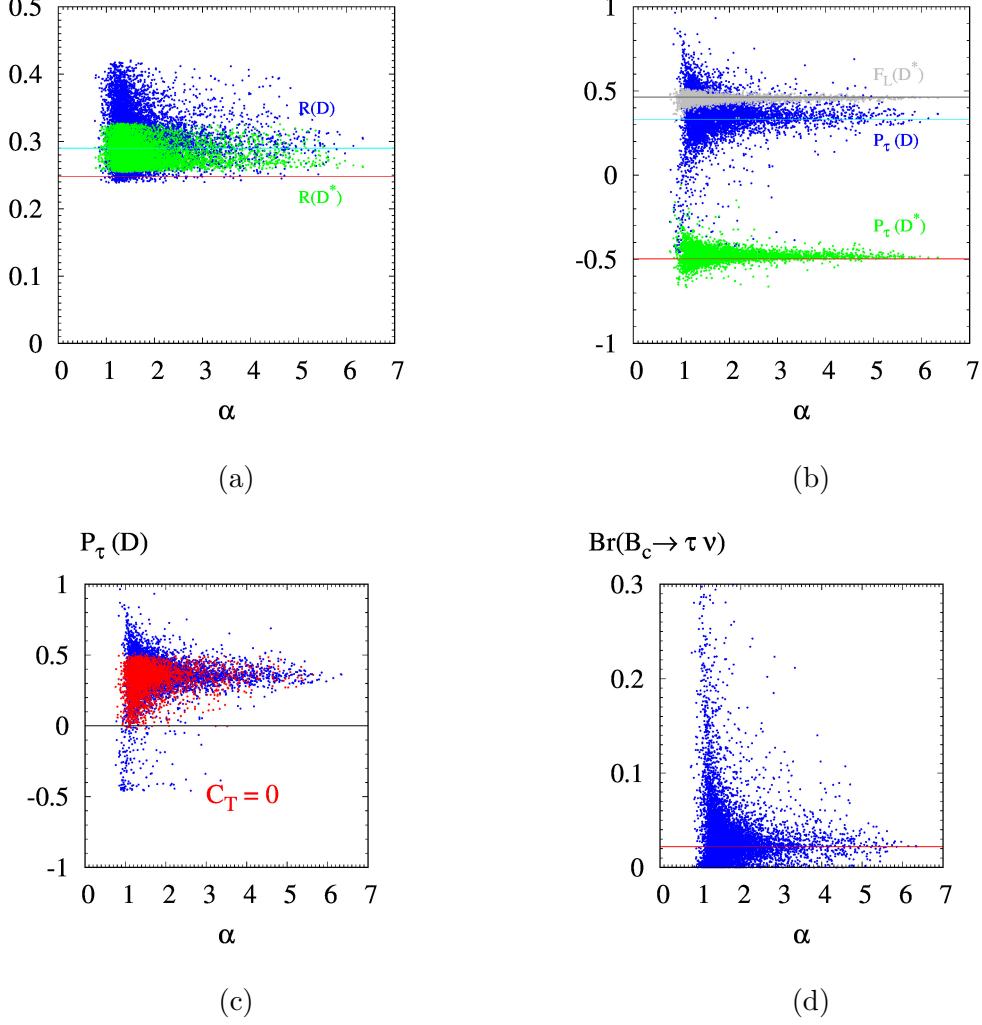


FIG. 3. Allowed regions of (a)  $R(D^{(*)})$ , (b)  $P_\tau(D^{(*)})$ ,  $F_L(D^{(*)})$ , (c)  $P_\tau(D)$  for  $C_T \neq 0$  (blue) and  $C_T = 0$  (red), and (d)  $\text{Br}(B_c \rightarrow \tau \nu)$  vs.  $\alpha$ , respectively, at the  $2\sigma$  level. In (a) cyan(red) line stands for the SM prediction of  $R(D)(R(D^{*}))$ ; in (b) grey, cyan, and red lines stand for the SM prediction of  $F_L(D^{*})$ ,  $P_\tau(D)$ , and  $P_\tau(D^{*})$ , respectively; in (d) red line is the SM prediction of the branching ratio.

where (A)  $C_{VL,SR} \neq 0$  and (B)  $C_{VL,SL,T} \neq 0$  allow negative  $P_\tau(D)$ . In case of (A) if  $C_T = 0$  then it is somewhat marginal such that almost all the allowed points of  $P_\tau(D)$  are positive and a few points are slightly negative; see Fig. 3 (c). If  $P_\tau(D)$  turned out to be negative, then it could restrict the shape of NP very strongly. Especially, if  $P_\tau(D)$  is negatively large, then  $C_T$  must be nonzero.

Figure 3 (c) shows that most of  $\text{Br}(B_c \rightarrow \tau \nu)$  values are safely less than  $\sim 0.1$ . Note that our constraint is  $\text{Br}(B_c \rightarrow \tau \nu) < 0.3$ . Since the SM value of the branching ratio ( $=0.022$ )

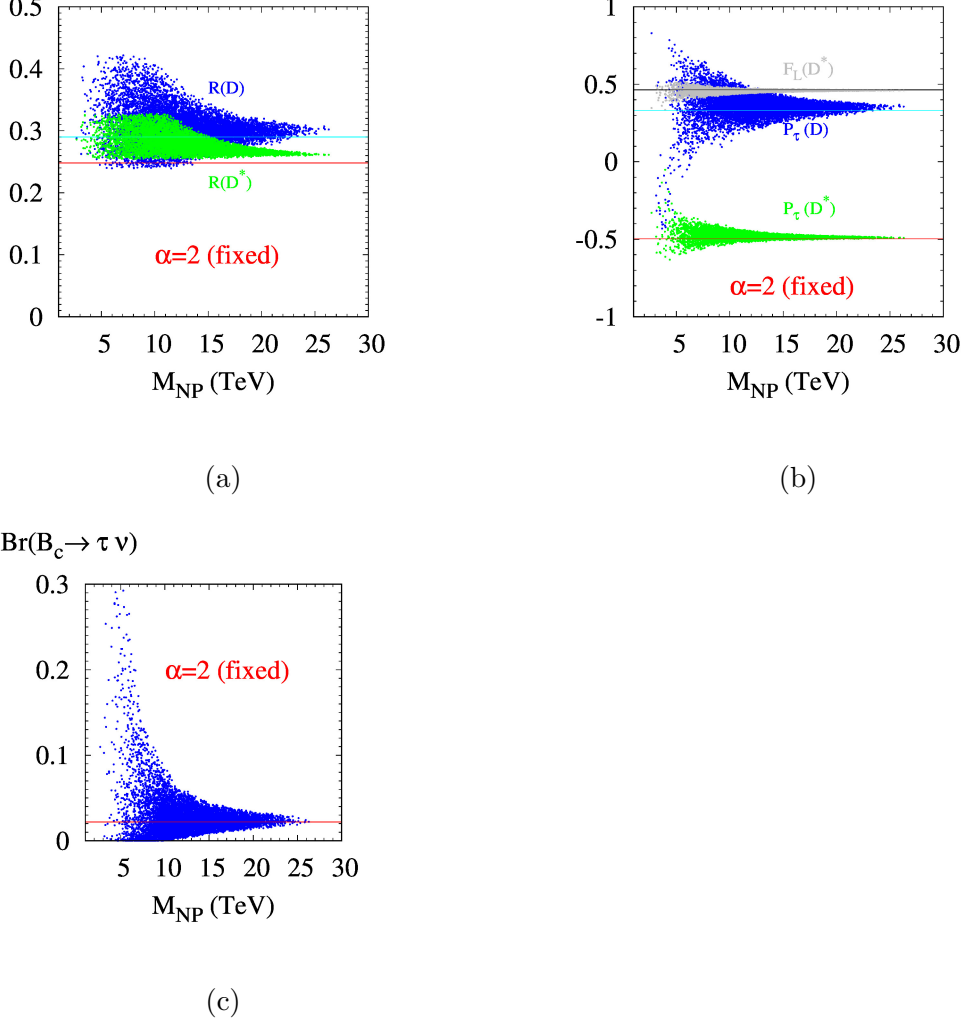


FIG. 4. Allowed regions of (a)  $R(D^{(*)})$ , (b)  $P_\tau(D^{(*)})$ ,  $F_L(D^*)$ , and (c)  $\text{Br}(B_c \rightarrow \tau \nu)$  vs.  $M_{\text{NP}}$ , respectively, at the  $2\sigma$  level for fixed  $\alpha = 2$ . In (a) cyan(red) line stands for the SM prediction of  $R(D)(R(D^*))$ ; in (b) grey, cyan, and red lines stand for the SM prediction of  $F_L(D^*)$ ,  $P_\tau(D)$ , and  $P_\tau(D^*)$ , respectively; in (c) red line is the SM prediction of the branching ratio.

is quite small compared to the upper limit, the constraint on the branching ratio is not so strong.

In Fig. 4 various observables are plotted with respect to  $M_{\text{NP}}$  for fixed  $\alpha = 2$ . All the observables shown tend to attenuate close to the SM values as  $M_{\text{NP}}$  gets larger. One can clearly see again that  $M_{\text{NP}} \lesssim 27$  TeV for  $\alpha = 2$ . For larger values of  $M_{\text{NP}}$ , NP effects get smaller and could not be compatible with the experimental data. The limiting case of  $M_{\text{NP}} \rightarrow \infty$  corresponds to the SM. Thus the upper bound of  $M_{\text{NP}}$  (for  $\alpha = 2$ ) indicates the existence of NP. The figures show that NP should exist to explain the experimental data in

case of  $\alpha = 2$ . For smaller  $\alpha \lesssim 1$ ,  $M_{\text{NP}}$  can be much larger (see Fig. 1) where NP effects would not be suppressed so much. As mentioned before, negative  $P_\tau(D)$  would indicate a strong evidence of NP. If NP is mediated by ordinary particles where  $\alpha = 2$  and  $P_\tau(D) < 0$ , then  $M_{\text{NP}}$  could not be larger than  $\simeq 6$  TeV as can be seen in Fig. 4 (b).

In Fig. 5 we plot the Wilson coefficients  $C_{VL,SL,SR,T}$ . Among 4 Wilson coefficients  $C_{VL,SL,SR,T}$  in our analysis two or three of them can be zero, but not all of them. It means that the SM where  $C_j = 0$  is not included in our allowed region at the  $2\sigma$ . In Fig 5 (d), straight lines represent  $C_{SL}(\mu_b) = +8.4C_T(\mu_b)$  and  $C_{SL}(\mu_b) = -8.9C_T(\mu_b)$ , which are inspired by the leptoquark model [45, 46]. As seen in Fig. 5 (d), our result prefers  $C_{SL} = -8.9C_T$ .

Figure 6 plots the Wilson coefficients vs.  $M_{\text{NP}}$  for the case of fixed  $\alpha = 2$ . The plots show a typical new-”particle” contribution of  $C_j \sim 1/M_{\text{NP}}^2$ . The  $M_{\text{NP}}$  dependences of  $C_{j \neq VL}$  involve the RG running effects. Comparing Fig. 6 (a) with (b) or (c), we find that the RG effects are not dominant. Again one can see that for fixed  $\alpha = 2$ ,  $M_{\text{NP}}$  can be as large as  $\sim 27$  TeV.

Figure 7 shows the allowed regions of some observables. As shown in Fig. 7 (a),  $R(D^*)$  has no overlaps with the SM. Figure 7 (b) provides allowed regions of polarization parameters  $P_\tau(D^{(*)})$  and  $F_L(D^*)$ . As discussed before  $P_\tau(D)$  is mostly positive but negative values are also possible. Figure 7 (c) shows the subregion of  $C_T = 0$  (red points). The NP scenario of  $C_T = 0$  with  $C_{VL,SR} \neq 0$  is very marginal. Figures 7 (d) and (e) plot the branching ratio  $\text{Br}(B_c \rightarrow \tau\nu)$  vs.  $R(D^{(*)})$ .

Figure 8 deals with  $R(J/\Psi)$  and  $R(\Lambda_c)$ . The best-fit values of our analysis are  $R(J/\Psi)_{\text{best-fit}} = 0.303$  and  $R(\Lambda_c)_{\text{best-fit}} = 0.379$ . The former is smaller than the experimental data while the latter larger, as the SM predictions. Our allowed regions are mostly deviated from the SM predictions, and  $R(\Lambda_c)$  has no overlaps with the SM. Figure 8 (b) plots  $R(\Lambda_c)$  vs.  $R(D^*)$ . Similar to previous observables,  $R(J/\Psi)$  and  $R(\Lambda_c)$  tends to get closer to the SM predictions as  $\alpha$  and  $M_{\text{NP}}$  (with fixed  $\alpha = 2$ ) gets larger as shown in Figs. 8 (c) and (d). Both of these two ratios have values in the vast majority slightly above the SM predictions. In Figs. 8 (e) and (f) we check the validity of the sum rule for  $R(\Lambda_c)$  in Eq. (14). Blue dots are from Eq. (26) while red ones from the sum rule. One can find that the sum rule works quite well. The reason is that the allowed range of  $|C_T|$  is much smaller than 1, and it ensures the validity of the sum rule as discussed in [4]. More data would check this feature and the consistency

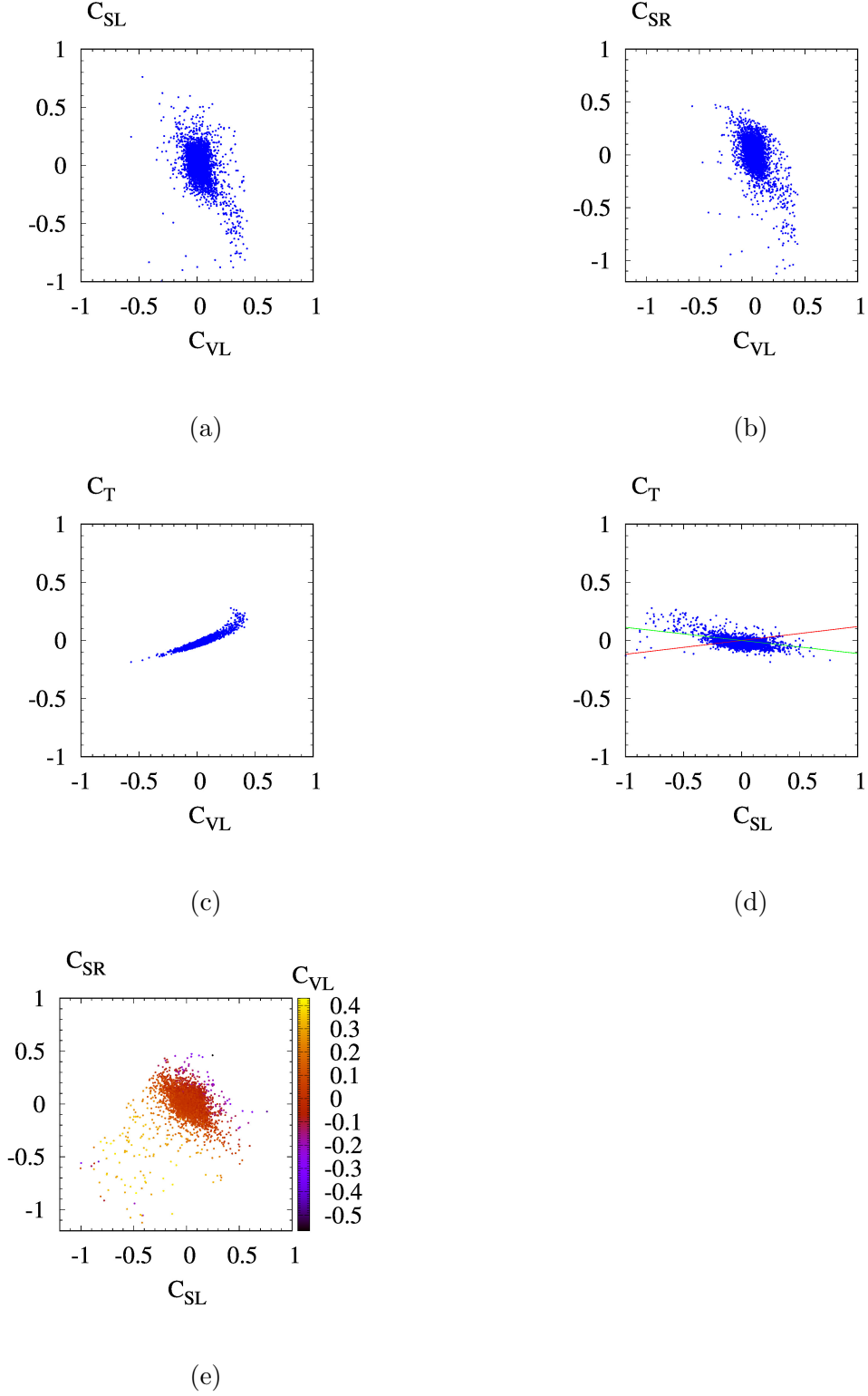


FIG. 5. Allowed regions of (a)  $C_{SL}$  vs.  $C_{VL}$ , (b)  $C_{SR}$  vs.  $C_{VL}$ , (a)  $C_T$  vs.  $C_{VL}$ , (b)  $C_T$  vs.  $C_{SL}$ , and (e)  $C_{SR}$  vs.  $C_{SL}$  with respect to  $C_{VL}^T$  at the  $2\sigma$  level. In (d), the red(green) line corresponds to  $C_{SL} = +8.4C_T(-8.9C_T)$  at  $\mu = \mu_b$ .

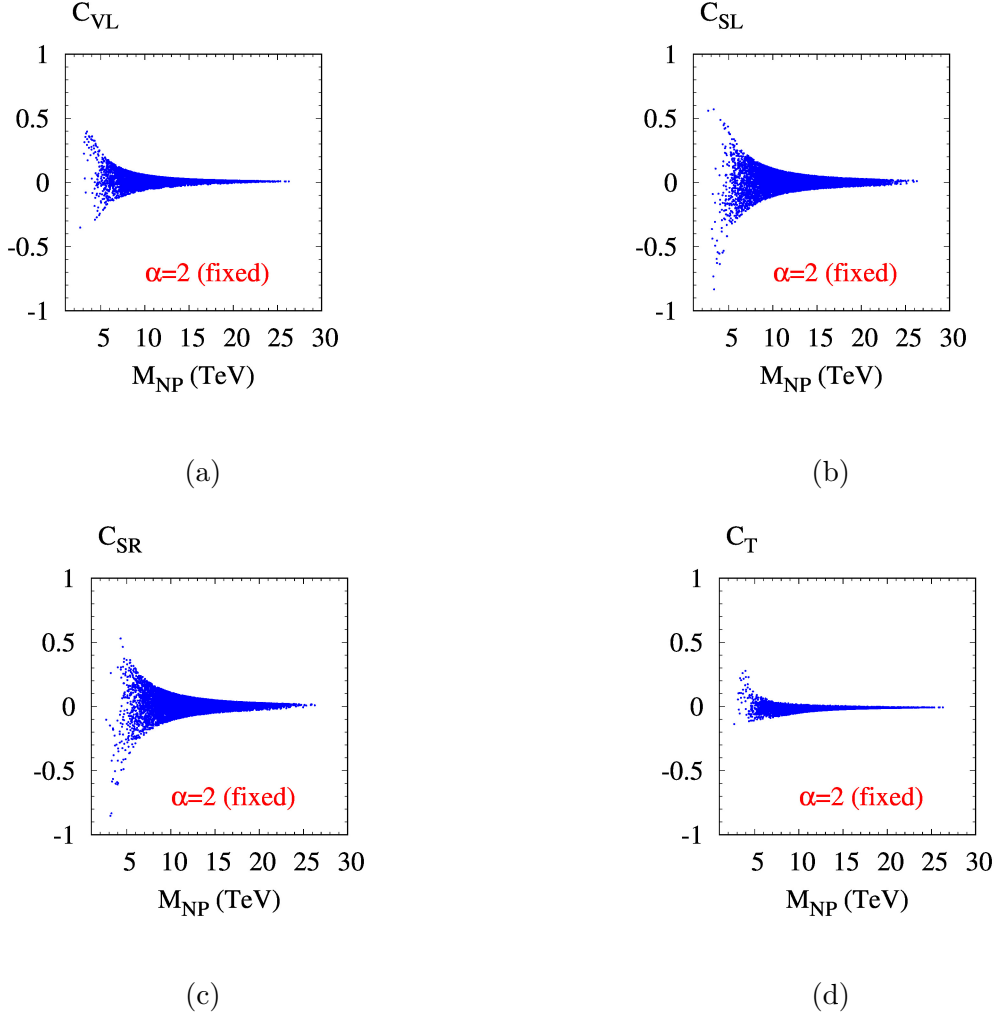
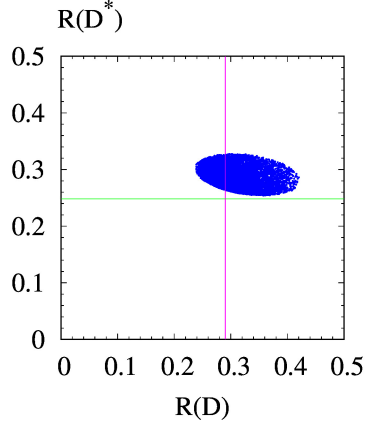


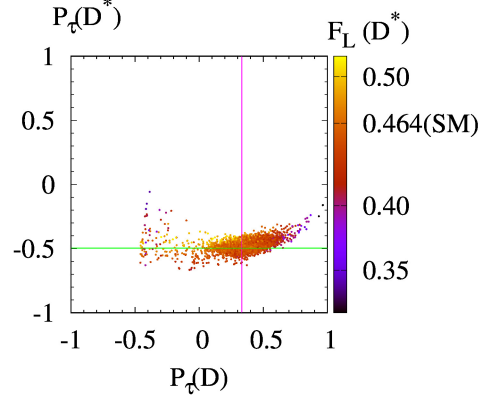
FIG. 6. Allowed regions of (a)  $C_{VL}$ , (b)  $C_{SL}$ , (c)  $C_{SR}$ , and (d)  $C_T$  vs.  $M_{NP}$ , respectively, at the  $2\sigma$  level for fixed  $\alpha = 2$ .

of the whole description for  $b \rightarrow c$  semi-leptonic decays.

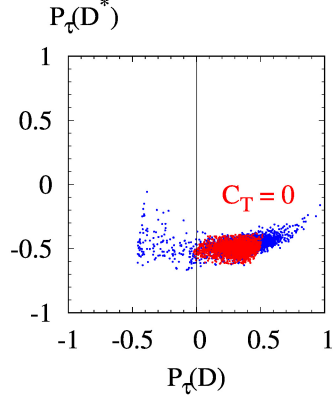
Final remarks are in order to discuss the theoretical implications of the parameter constraints. Our analysis can be used to check the validity of certain NP scenarios in a generic way with respect to  $b \rightarrow c\tau\nu$  decays. As an example, for a weak doublet scalar LQ  $R_2$ , one has  $A_{SL}^{R_2} = y_2^{LR}(y_2^{RL})^*/(2V_{cb})$  [3] where  $y_2^{AB}$  are the relevant couplings. For order one couplings the mass of  $R_2$  is required to go over 20 TeV by the  $b \rightarrow s$  data. Similar analysis shows that the mass of the vector weak doublet LQ  $V_2$  should be larger than 30 TeV [3]. This is quite challenging because our analysis requires  $M_{NP} \lesssim 27$  TeV for  $|A_j| \leq 100$ . On the other hand, for the scalar weak triplet LQ  $S_3$  and the vector weak triplet LQ  $U_3$  with order one couplings, the lower bound of the LQ scale is about 50 TeV by  $b \rightarrow s$  data [3].



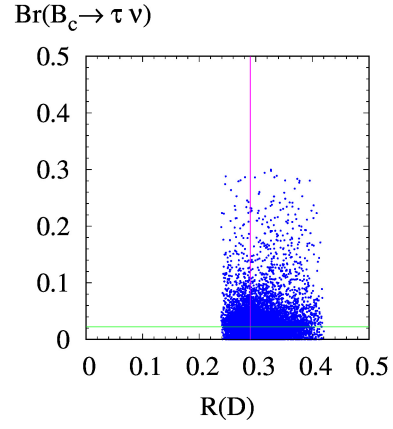
(a)



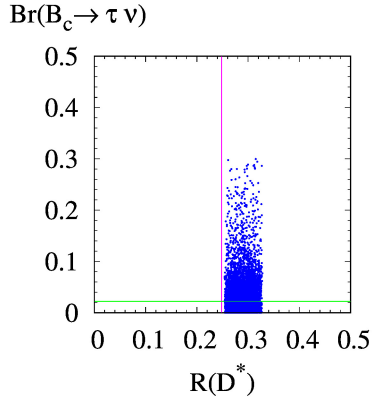
(b)



(c)



(d)



(e)

FIG. 7. Allowed regions of (a)  $R(D^*)$  vs.  $R(D)$ , (b)  $P_\tau(D^*)$  vs.  $P_\tau(D)$  with respect to  $F_L(D^*)$ , (c)  $P_\tau(D^*)$  vs.  $P_\tau(D)$  for  $C_T \neq 0$  (blue) and  $C_T = 0$  (red), (d)  $\text{Br}(B_c \rightarrow \tau \nu)$  vs.  $R(D)$ , and (e)  $\text{Br}(B_c \rightarrow \tau \nu)$  vs.  $R(D^*)$  at the  $2\sigma$  level. Green and magenta lines are the SM predictions.

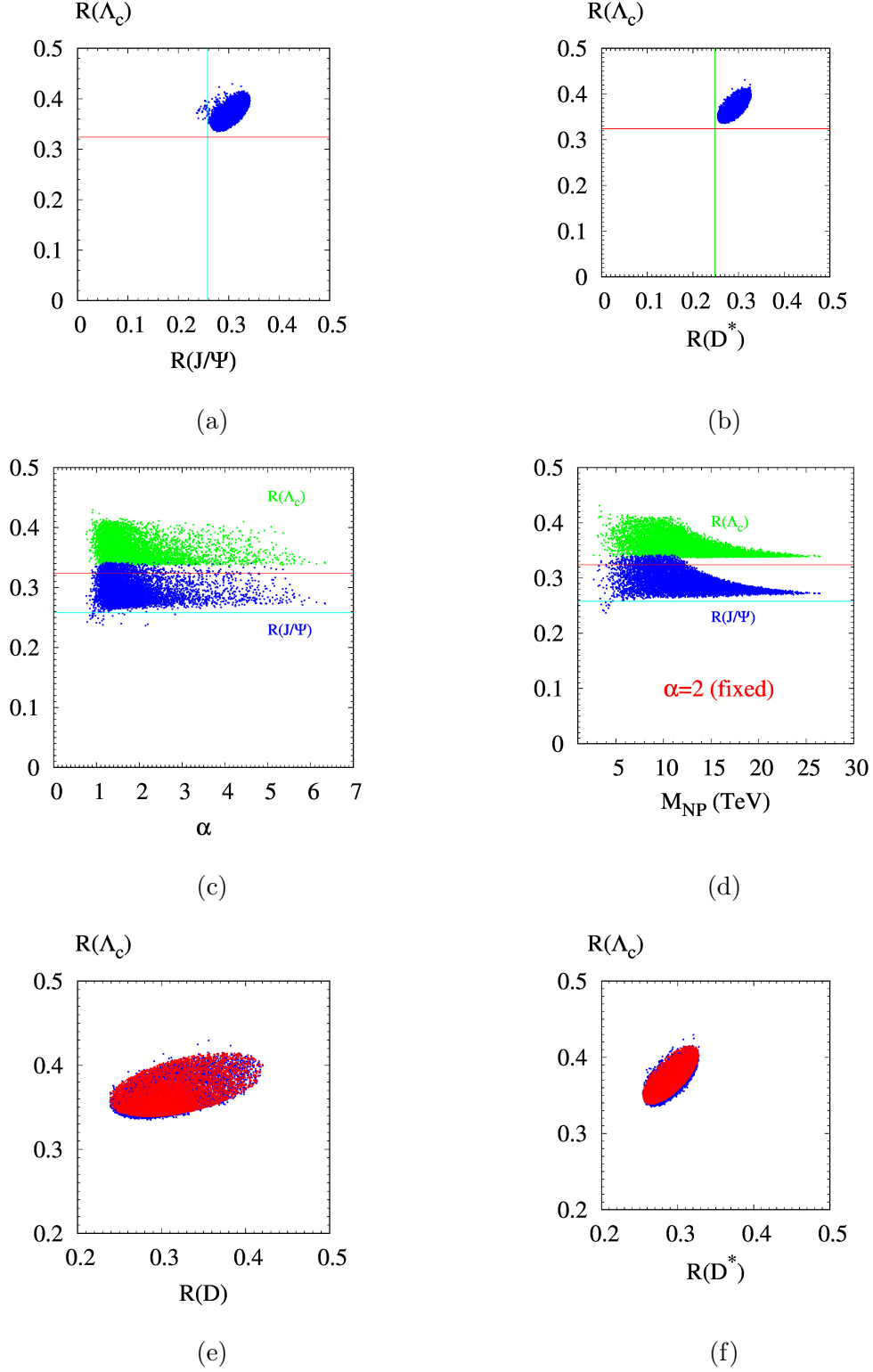


FIG. 8. Allowed regions of (a)  $R(\Lambda_c)$  vs.  $R(J/\Psi)$ , (b)  $R(\Lambda_c)$  vs.  $R(D^*)$  (c)  $R(J/\Psi)$  and  $R(\Lambda_c)$  vs.  $\alpha$ , (d)  $R(J/\Psi)$  and  $R(\Lambda_c)$  vs.  $M_{\text{NP}}$  for fixed  $\alpha = 2$ , (e)  $R(\Lambda_c)$  vs.  $R(D)$  from Eq. (26) (blue) and from the sum rule of Eq. (14), and (f)  $R(\Lambda_c)$  vs.  $R(D^*)$  from Eq. (26) (blue) and from the sum rule of Eq. (14), at the  $2\sigma$  level. Straight lines are the SM predictions for  $R(J/\Psi)$  (cyan),  $R(\Lambda_c)$  (red), and  $R(D^*)$  (green) .



According to our analysis,  $S_3$  and  $U_3$  are not compatible with  $b \rightarrow c$  transition. For other NP models one can do the similar estimations to support or disfavor the model.

In addition, as discussed before, negative  $P_\tau(D)$  if observed would strongly constrain the Lorentz structure of NP such that  $C_{VL,SR} \neq 0$  or  $C_{VL,SL,T} \neq 0$ . The last term of  $P_\tau(D)$  in Eq. (22),  $-1.09(1 + C_{VL})C_T^*$  plays an important role, and negatively large  $P_\tau(D)$  requires  $C_T \neq 0$ .

#### IV. CONCLUSIONS

In conclusion we investigated possible NP effects at tree level on  $B \rightarrow D^{(*)}\ell\nu$  decays with operators  $\mathcal{O}_{VL,SL,SR,T}$ . Corresponding Wilson coefficients  $C_j$  are parameterized by a new NP scale  $M_{\text{NP}}$  and its power with fermionic couplings  $A_j$ . Allowed regions of  $|C_T|$  are narrower than other Wilson coefficients  $|C_{VL,SL,SR}|$ . The analysis was done for  $-100 \leq A_j \leq 100$ . Within this range we found that the NP scale is  $M_{\text{NP}} \lesssim 27$  TeV for ordinary new particles where  $\alpha = 2$ . One should keep in mind that if  $|A_j|$  could be larger, then bounds on  $M_{\text{NP}}$  discussed above can also be larger accordingly. Conversely, current accelerator energy is quite below 27 TeV so that only the region of small  $|A_j|$  could be investigated experimentally.

The ratio  $R(D^*)$  turned out to be still far away from the SM. In our framework the polarization asymmetry  $P_\tau(D)$  can have negative values while the SM prediction of it is positive. We found that negative  $P_\tau(D)$  is possible for  $\mathcal{O}_{VL,SR} \neq 0$  or  $\mathcal{O}_{VL,SL,T} \neq 0$ , and models with  $(\mathcal{O}_{VL,SR} \neq 0, \mathcal{O}_T = 0)$  is marginal. If  $P_\tau(D)$  turned out to be negatively large, then  $C_T$  should be nonzero. Also, negative  $P_\tau(D)$  would impose a strong bound on the NP scale as  $M_{\text{NP}} \lesssim 6$  TeV for  $\alpha = 2$ . Thus the measurement of  $P_\tau(D)$  would be very interesting in probing the NP structure.

In our analysis  $R(J/\Psi)$  has slight overlaps with SM while  $R(\Lambda_c)$  does not. We checked that the sum rule for  $R(\Lambda_c)$  with respect to  $R(D^{(*)})$  works very well thanks to small values of  $|C_T|$ .

In specific models, one should consider many other constraints from processes such as  $B \rightarrow DD$  decay,  $B_s \rightarrow \mu\mu$  decay,  $B_{(s)}\bar{B}_{(s)}$  mixing, and so on. The results would directly affect  $A_j$  and possibly  $\alpha$ . Our framework could provide more general ways to handle various kinds of NP scenarios, and check whether we would support or exclude certain NP models.

## ACKNOWLEDGMENTS

This paper was supported by Konkuk University in 2024.

---

- [1] R. Aaij *et al.* [LHCb], Phys. Rev. Lett. **131**, no.5, 051803 (2023).
- [2] R. Aaij *et al.* [LHCb], Phys. Rev. D **108**, no.3, 032002 (2023).
- [3] A. D’Alise, G. Fabiano, D. Frattulillo, D. Iacobacci, F. Sannino, P. Santorelli and N. Vignaroli, Nucl. Phys. B **1006**, 116631 (2024).
- [4] S. Iguro, T. Kitahara and R. Watanabe, Phys. Rev. D **110**, no.7, 7 (2024).
- [5] LHCb Collaboration, “ $b \rightarrow cl\nu$  decays at LHCb.”.  
[https://indico.in2p3.fr/event/32664/timetable/?view=standard\\_numbered#38-b-to-c-l-nu-decays-at-lhcb](https://indico.in2p3.fr/event/32664/timetable/?view=standard_numbered#38-b-to-c-l-nu-decays-at-lhcb).
- [6] S. Hirose *et al.* [Belle Collaboration], Phys. Rev. Lett. **118**, no. 21, 211801 (2017).
- [7] S. Hirose *et al.* [Belle Collaboration], Phys. Rev. D **97**, no. 1, 012004 (2018).
- [8] R. Aaij *et al.* [LHCb], Phys. Rev. D **110**, no.9, 092007 (2024).
- [9] A. Abdesselam *et al.* [Belle Collaboration], arXiv:1903.03102 [hep-ex].
- [10] Y. Sakaki, M. Tanaka, A. Tayduganov and R. Watanabe, Phys. Rev. D **88**, no.9, 094012 (2013).
- [11] M. Freytsis, Z. Ligeti and J. T. Ruderman, Phys. Rev. D **92**, no.5, 054018 (2015).
- [12] M. Bauer and M. Neubert, Phys. Rev. Lett. **116**, no.14, 141802 (2016).
- [13] S. Fajfer and N. Košnik, Phys. Lett. B **755**, 270-274 (2016).
- [14] D. Bečirević, S. Fajfer, N. Košnik and L. Pavičić, Phys. Rev. D **110**, no.5, 5 (2024).
- [15] B. Bhattacharya, A. Datta, D. London and S. Shivashankara, Phys. Lett. B **742**, 370-374 (2015).
- [16] A. Greljo, G. Isidori and D. Marzocca, JHEP **07**, 142 (2015).
- [17] S. M. Boucenna, A. Celis, J. Fuentes-Martin, A. Vicente and J. Virto, JHEP **12**, 059 (2016).
- [18] M. Carena, E. Megías, M. Quíros and C. Wagner, JHEP **12**, 043 (2018).
- [19] S. Fajfer, J. F. Kamenik, I. Nisandzic and J. Zupan, Phys. Rev. Lett. **109**, 161801 (2012).
- [20] A. Crivellin, C. Greub and A. Kokulu, Phys. Rev. D **86**, 054014 (2012).
- [21] A. Celis, M. Jung, X. Q. Li and A. Pich, JHEP **01**, 054 (2013).

- [22] J. P. Lee, Mod. Phys. Lett. A **36**, no.30, 2150219 (2021).
- [23] J. P. Lee, J. Korean Phys. Soc. **80**, no.1, 13-19 (2022).
- [24] J. P. Lee, Mod. Phys. Lett. A **38**, no.16n17, 2350080 (2023).
- [25] M. Blanke, A. Crivellin, S. de Boer, T. Kitahara, M. Moscati, U. Nierste and I. Nišandžić, Phys. Rev. D **99**, no.7, 075006 (2019).
- [26] M. Blanke, A. Crivellin, T. Kitahara, M. Moscati, U. Nierste and I. Nišandžić, Phys. Rev. D **100**, no.3, 035035 (addendum, 2019).
- [27] M. Fedele, M. Blanke, A. Crivellin, S. Iguro, T. Kitahara, U. Nierste and R. Watanabe, Phys. Rev. D **107**, no.5, 055005 (2023).
- [28] J. Harrison *et al.* [LATTICE-HPQCD], Phys. Rev. Lett. **125**, no.22, 222003 (2020).
- [29] F. U. Bernlochner, Z. Ligeti, D. J. Robinson and W. L. Sutcliffe, Phys. Rev. Lett. **121**, no.20, 202001 (2018).
- [30] F. U. Bernlochner, Z. Ligeti, D. J. Robinson and W. L. Sutcliffe, Phys. Rev. D **99**, no.5, 055008 (2019).
- [31] F. U. Bernlochner, Z. Ligeti, M. Papucci and D. J. Robinson, Phys. Rev. D **107**, no.1, L011502 (2023).
- [32] R. Alonso, B. Grinstein and J. Martin Camalich, Phys. Rev. Lett. **118**, no.8, 081802 (2017).
- [33] S. Aoki *et al.*, Eur. Phys. J. C **77**, no. 2, 112 (2017).
- [34] F. U. Bernlochner, Z. Ligeti, M. Papucci and D. J. Robinson, Phys. Rev. D **95**, no. 11, 115008 (2017) Erratum: [Phys. Rev. D **97**, no. 5, 059902 (2018)].
- [35] J. P. Lees *et al.* [BaBar Collaboration], Phys. Rev. D **88**, no. 7, 072012 (2013).
- [36] M. Huschle *et al.* [Belle Collaboration], Phys. Rev. D **92**, no. 7, 072014 (2015).
- [37] Y. Sato *et al.* [Belle Collaboration], Phys. Rev. D **94**, no. 7, 072007 (2016).
- [38] S. Hirose [Belle Collaboration], Nucl. Part. Phys. Proc. **287-288**, 185 (2017).
- [39] A. Abdesselam *et al.* [Belle Collaboration], arXiv:1904.08794 [hep-ex].
- [40] I. Adachi *et al.* [Belle-II], Phys. Rev. D **110**, no.7, 072020 (2024).
- [41] R. Aaij *et al.* [LHCb Collaboration], Phys. Rev. Lett. **115**, no. 11, 111803 (2015) Addendum: [Phys. Rev. Lett. **115**, no. 15, 159901 (2015)].
- [42] R. Aaij *et al.* [LHCb Collaboration], Phys. Rev. D **97**, no. 7, 072013 (2018).
- [43] R. Aaij *et al.* [LHCb], Phys. Rev. D **108**, no.1, 012018 (2023) [erratum: Phys. Rev. D **109**, no.11, 119902 (2024)].

- [44] Average of  $R(D)$  and  $R(D^*)$  for Spring 2019, Heavy Flavor Averaging Group, <https://hflav-eos.web.cern.ch/hflav-eos/semi/spring19/html/RDsDsstar/RDRDs.html>
- [45] S. Iguro, T. Kitahara and R. Watanabe, [arXiv:2210.10751 [hep-ph]].
- [46] B. Capdevila, A. Crivellin and J. Matias, Eur. Phys. J. ST **1**, 20 (2023).